2015

Automating and Calibrating a Scanning Tunneling Microscope for Use in an Advanced Laboratory Course

Spencer Fuller
University of Redlands

Automating and Calibrating a Scanning Tunneling Microscope for Use in an Advanced Laboratory Course

Spencer Fuller

April 16, 2015

Abstract

University of Redlands student Jonathan Paez and I worked on automating and calibrating a student constructed scanning tunneling microscope (STM) with the intention of using it for pedagogical purposes in an advanced laboratory course. We automated the STM by incorporating a linear actuator and labVIEW. We were successful in creating three dimensional plots of graphite and gold surfaces and deriving calibrations to convert our data from voltages to distances. We discovered that our STM has nanometer-scale resolution.

1   Introduction

In 1981, Gerd Binnig and Heinrich Rohrer developed the scanning tunneling microscope (STM).[1] Five years later they were awarded the Nobel Prize in Physics. The scanning tunneling microscope has since become widely used by surface scientists in areas such as materials science, biology, organic chemistry, and catalysis.[2,3]

Scanning tunneling microscopes are part of a family of scanning probe microscopes, which allow the user to construct a topographical map of a surface on the nanometer or atomic scale. STMs are frequently used over other probing microscopy methods because of their superior resolution. Most STMs are able to achieve atomic resolution while other types of microscopes such as the field ion microscope or reflection electron microscope are only able to achieve nanometer scale resolution.[4] STMs are frequently used in the development of nanotechnology and in the study of surface chemistry and surface morphology. For example, scientists have been able to detect which atoms have reacted to a substrate using the STM.[5] The STM also has applications in biology such as determining structures of nucleic acids and proteins.[6] Unfortunatley, the STM can only scan conductive surfaces. Other microscopes must be used when scanning nonconductive surfaces.

Researchers are able to use STMs to view surface features such as atomic structures and defects. For example, scientists have used STMs to characterize defects and roughness on superconductors.[7] Scientists have even used STMs to move individual atoms to build atomic structures. They explain that the process of transporting atoms or molecules across a surface is analogous to the

operation of a crane at a construction site.[8] The STM is very versatile. In the past 34 years since its creation, surface scientists have been using STMs in many different fields and in a variety of environments ranging from ultra high vacuum to sub-Kelvin temperatures.

I will describe how we automated and calibrated an STM to make it more user-friendly. The STM was buiilt by Chris Adams, a previous University of Redlands research student. First, I will discuss the theory behind quantum tunneling and how the STM exploits this phenomenon to obtain images of surfaces at the atomic scale. Then I will discuss the mechanics of the STM, some of its limitations, and the necessary precautions when designing STMs. Next I will describe how we automated our STM using a linear actuator and LabVIEW. Finally, I will present a derivation of the calibration process to convert the voltage measurements into distances and the results from scans using graphite and gold surfaces.

2 Theory

2.1 Quantum Tunneling

I will present three different approximations to model the tunneling of electrons between the sample and the tip. The approximations from simplest to most complex are: the finite square well, the WKB approximation, and the Bardeen approach.

2.1.1 Finite Square Well

We begin with the one-dimensional time-independent Schrödinger equation, which describes the wavefunction of a particle of mass m,

$$-\frac{\hbar^2}{2m}\frac{d^2\psi(z)}{dz^2} + U(z)\psi(z) = E\psi(z). \tag{1}$$

Although our STM is an open-air STM, we can approximate the gap between the tip and the sample as a vacuum. We can simplify the tunneling process by approximating the potential across the gap as a finite square barrier potential instead of the sloped potential shown in Figure 1.
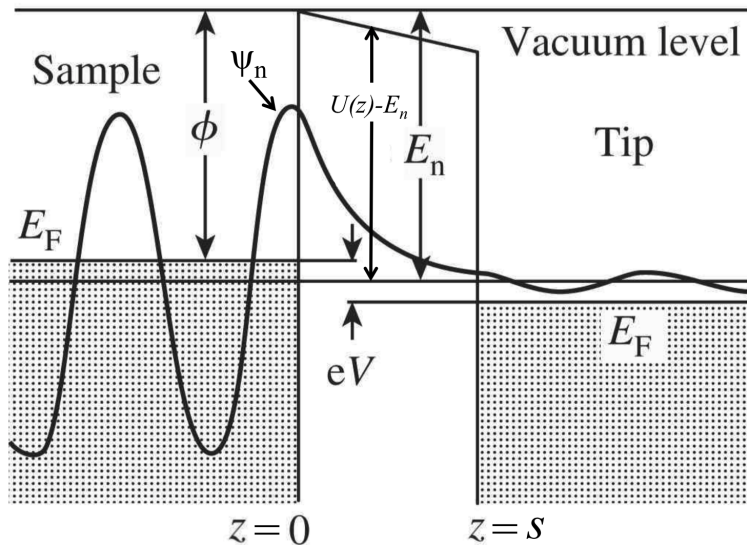
Figure 1: A sloped finite square barrier potential representation of the tip-sample separation.[10]

We will consider the scattering states, that is, those states with $E > U$. In the region where $z < 0$, $U = 0$, so

$$\frac{d^2\psi}{dz^2} = -k^2\psi, \tag{2}$$

where $k \equiv \frac{\sqrt{2mE}}{\hbar}$. This has the general solution $\psi(z) = Ae^{-ikz} + Be^{ikz}$. The solution will oscillate for $E > U$ because of the imaginary exponentials. Similarly, in the region where $z > s$ the solution is $\psi(z) = Ee^{-ikz} + Fe^{ikz}$. We are going to assume that waves are coming in from a single direction. This turns out to be a good assumption because the bias voltage on the STM allows us to increase the number of electrons tunneling through the barrier in a certain direction. In the region where $0 < z < s$, $E < U$. Solving the Schrödinger equation in this region gives $\psi(z) = Ce^{-lz} + De^{lz}$, where $l \equiv \frac{\sqrt{2m(U-E)}}{\hbar}$. The solution will decay exponentially.

We have found the general solutions to the Schrödinger equation for each of the regions. To find particular solutions we must use the boundary conditions. At each boundary ($z = 0$ or $z = s$), $\psi(z)$ and $\frac{d\psi(z)}{dz}$ must be continuous. Thus, we get the following four equations after evaluating the solutions and their derivatives at $z = 0$ and $z = s$:

$$A + B = C + D, \tag{3}$$

$$ik(A + B) = l(-C + D), \tag{4}$$

$$Ce^{-ls} + De^{ls} = Fe^{-iks} + Ge^{iks}, \tag{5}$$

3

$$l(-Ce^{-ls} + De^{ls}) = ik(-Fe^{-iks} + Ge^{iks}). \tag{6}$$

We will assume that $F = 0$ so that there is no incoming wave from the right. The transmission coefficient is given by $T = \frac{|G|^2}{|A|^2}$. Solving for G and A using Equations 3-6 and substituting gives[11]

$$T = \frac{1}{1 + \frac{U^2}{4E(E+U)} \sin^2\left(\frac{2s}{\hbar}\sqrt{2m(E+U)}\right)}. \tag{7}$$

Using the identity $\sinh(x) = \frac{1}{2}(e^x - e^{-x})$, Equation 7 simplifies to

$$T = \frac{1}{1 + \frac{U^2}{4E(U-E)}\frac{1}{4}(e^\gamma - e^{-\gamma})^2}, \tag{8}$$

where $\gamma \equiv \frac{2s}{\hbar}\sqrt{2m(U-E)}$. We can simplify further if we assume $T << 1$ (the fraction of particles that make it through is very small). The negative exponential in the denominator goes to 0 and T simplifies to

$$T \approx \frac{1}{1 + \frac{e^{2\gamma}U^2}{16E(U-E)}} \approx \frac{16E(U-E)}{U^2}e^{-2\gamma}. \tag{9}$$

The transmission coefficient T is exponentially related to the tip-sample separation s because γ is linearly related to s. Given a typical value for $U - E$ of 4 to 5 eV, a change in separation of about half an angstrom yields a 10% change in the transmission coefficient. This is a significant fraction of the tunneling signal from a very small change in separation (smaller than our STM can control).

2.1.2   WKB Approximation

Using the WKB approximation, a technique for obtaining solutions to the time-independent Schrödinger equation by approximating the potential as a function of position instead of constant where $0 < z < s$,[12]

$$T \approx e^{-2\gamma'}, \text{ with } \gamma' \equiv \frac{1}{\hbar}\int_0^s |p(z)|dz \text{ and } p(x) \equiv \sqrt{2m[E - U(z)]}. \tag{10}$$

Approximating the potential as having a constant slope between the gap, we can write down an expression for $U(z)$ and integrate to find γ'. From Figure 1 we find $U(z) - E = \phi - \frac{zeV}{s}$. Substituting into Equation 10 yields

$$\gamma' = \frac{2s\sqrt{2m}}{3eV\hbar}\left((eV - \phi)^{3/2} - \phi^{3/2}\right). \tag{11}$$

Equation 11 shows that γ' is linearly dependent on the tip-sample separation and thus the transmission coefficient is nearly exponentially related to the separation.

2.1.3 Bardeen Approach

The previous two methods described how the transmission coefficient is related to the separation. The Bardeen approach will be able to quantify a current and give a more accurate description of tunneling because it will allow the electrons in the tip and sample to be in different states. For a tunneling current to flow, an electron must flow from a state in the sample with energy E_μ to a state in the tip with energy E_v. The tunneling current will depend on how occupied the state is in the sample, $f(E_\mu)$, and how unoccupied the state is in the tip, $1 - f(E_v + eV)$. It will also depend on the separation between the tip and sample. The tunneling current given by first-order perturbation theory is

$$I = \frac{2\pi e}{\hbar} \Sigma_{\mu v} f(E_\mu)[1 - f(E_v + eV)] \times |M_{\mu v}|^2 \delta(E_\mu - E_v), \qquad (12)$$

where $f(E)$ is the Fermi function, V is the applied voltage, and $M_{\mu v}$ is the tunneling matrix element between states.[13] δ is the Kronecker delta function, which equals 1 when $E_\mu = E_v$ and equals 0 when $E_\mu \neq E_v$. The Fermi function is the probability a given available state will be occupied at temperature T. The tunneling matrix is a measure of how much the wavefunctions of the electrons on the tip and wavefunctions of the electrons on the sample overlap, thus the tip-sample separation. It describes the transition of an electron in state a ψ_μ to a state ψ_v. It has units of energy and physically represents the energy lowering due to the overlap of the two states.[14] Bardeen[15] has shown that the tunneling matrix element is given by

$$M_{\mu,v} = \frac{\hbar^2}{2m} \int d\vec{S} \cdot (\psi_\mu^* \vec{\nabla} \psi_v - \psi_v \vec{\nabla} \psi_\mu^*), \qquad (13)$$

where $d\vec{S}$ is a differential piece of surface, and ψ_μ and ψ_v are the wavefunctions of the sample and tip respectively. Equations (12) and (13) are sometimes referred to as the transfer Hamiltonian theory. The tunneling matrix is reminiscent of the probability current, which in one dimension is defined as $J(x,t) \equiv \frac{i\hbar}{2m} \left(\Psi \frac{\delta \Psi^*}{\delta x} - \Psi^* \frac{\delta \Psi}{\delta x} \right)$. The probability current tells you the rate at which probability is flowing past a point x.

Tersoff and Hamann have also shown that[16]

$$|\psi_v(\vec{r}_0)|^2 \propto e^{-2\kappa(R+d)}. \qquad (14)$$

Equation 14 shows an exponential dependence on the tip-sample separation. Modeling the tip state as a modified hydrogen 1s state and assuming the sample has a periodic lattice, J. Tersoff and D. R. Hamann have evaluated $M_{\mu,v}$ and shown that

$$I = 32\pi^3 \hbar^{-1} e^2 V \phi^2 D_t(E_F) R^2 \kappa^{-4} e^{2\kappa R} \times \sum_v |\psi_v(\vec{r}_0)|^2 \delta(E_v - E_F), \qquad (15)$$

where $\kappa \equiv \sqrt{\frac{2m\phi}{\hbar^2}}$, ϕ is the work function, R is the radius of curvature of the tip, D_t is the density of states per unit volume of the probe tip, and $\vec{r}_0$ is the position of the center of curvature of the tip. The work function is the barrier

height, or the amount of work needed to remove an electron from the tip. The density of states is a measure of the number of available states at an energy an electron can occupy. From Equations 14 and 15, we see that the tunneling current is exponentially related to the separation,

$$I \propto e^{-2\kappa d}. \tag{16}$$

Equation 16 is similar in form to Equation 9 and Equation 10. Figure 2 shows a comparison of the WKB approximation and the Bardeen approach for different barrier heights. Tunneling is different for low barriers and high barriers. Transmission through low barriers is ballistic transport, while transmission through high barriers is tunneling. For thin barriers, these two mechanisms of transmission are qualitatively the same.
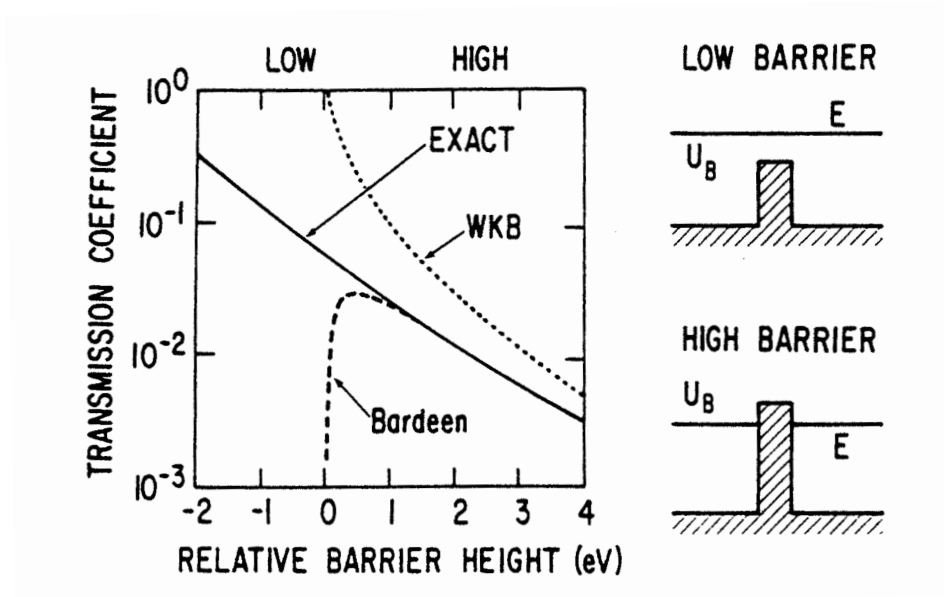

Figure 2: A comparison of two of the types of tunneling theories described above.[18]

2.2   Scanning Tunneling Microscopy

The scanning tunneling microscope works by scanning a very sharp tip across a surface while measuring changes in the current that tunnels between the sample and tip. We saw above that the current is extremely sensitive to the tip-sample separation.

There are two methods for scanning. The first is the constant height method. In this method the tip is scanned across the surface at a constant height and changes in the tunneling current are measured. Figure 3(a) shows how the

current responds to changes in the surface height. The current will increase when the tip passes over a higher surface feature and will decrease when it passes over a lower surface feature. Unfortunately, this method could lead to the tip crashing into surface features. Though this method allows for quicker scans, it is not as reliable. The method that Chris Adams used for our STM is the constant current method. In this method the tip is scanned across the surface so that the separation between the tip and sample remains constant throughout the scan, as illustrated in Figure 3(b). In order for the tip to maintain this distance, the STM needs a feedback loop to tell the tip to move backward if it's too close, or forward if it's too far. Because the movements of the tip take finite amounts of time, the STM must scan at a slower rate in order to allow the tip to move and maintain its resolution.
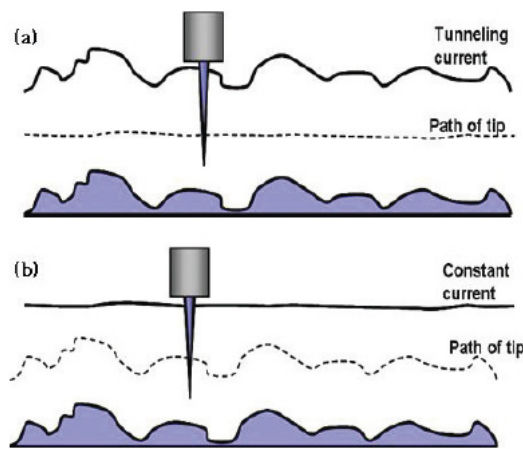

Figure 3: The two types of scanning. (a) Constant height mode. (b) Constant current mode.[20]

The STM uses a piezo to control the tip. A piezo is an electric device that deforms when a voltage is applied to it. This allows control of the tip in the x, y, and z directions. The piezo we are using in our STM is able to move the tip on the order of microns. Research grade STMs usually have piezos with much finer control to obtain an image with atomic resolution. A variety of shapes can be used for the piezo such as a tube, tripod, or disk. Chris Adams incorporated a disk piezo into our STM.

In order to create three dimensional surface plots, we need to scan in two directions. A sawtooth voltage controls scanning in the x direction while a slower ramp voltage controls scanning in the y direction. These are shown in Figures 4(a) and 4(b). Together, they result in the tip tracing a zig-zag pattrn across the surface. In practice, the ramp voltage is very slow and the pattern is much tighter than in Figure 4(c).
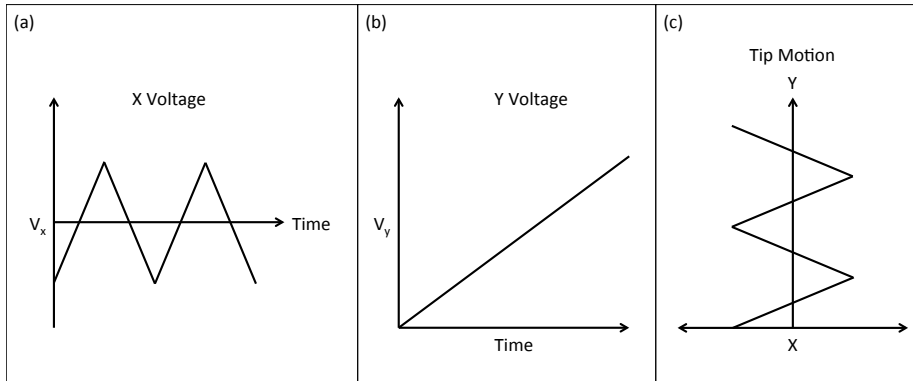
Figure 4: (a) A sawtooth voltage controls the motion in the x direction. (b) A ramp voltage controls the motion in the y direction. (c) The resulting motion is a zig-zag across the surface.

In order to achieve the best possible resolution, the STM must be isolated from all vibrations. This is especially important when achieving atomic resolution. Given that the typical corrugation amplitude is 0.1 Å for atomic resolution, vibrations must be reduced to less than 0.01 Å.[21] Typical STMs use springs as a source of vibration isolation. Our STM is situated on an optics table which floats when its legs are filled with air.

3   Mechanical Design

Our STM consists of two plates separated by three screws as shown in Figure 5. This setup is called a kinematic mount. The coarse approach screws lower the right side of the plate and lower the tip on the order of microns. The fine approach screw lowers the left side of the plate and lowers the tip on the order of angstroms.
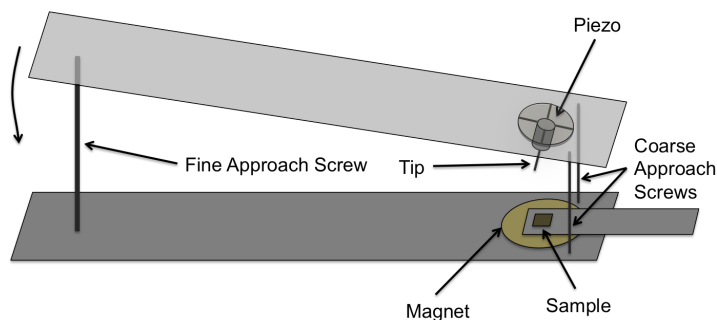

Figure 5: Diagram of STM.

To begin a scan, we lower the top plate using the coarse approach screws until we can barely discern the separation between the tip and the sample using a magnifying glass. Next, we use a fine approach screw to lower the tip even further to a few angstroms above the surface. Chris Adams designed the STM

8

with a manual fine approach screw. This led to many tip crashes and the automation of the approach process.

4 Automation

We automated the STM in two ways. First, we incorporated a linear actuator. Second, we wrote a program in LabVIEW to control the linear actuator and automate the approach process.

4.1 Linear Actuator

We replaced the fine approach screw with a linear actuator to move the tip down into the scanning position. A linear actuator is a device that moves a metal tip up or down on the order of tenths of microns. The linear actuator raises and lowers the top plate as seen in Figure 8. It is capable of moving $0.1\mu m$ per step, which translates to a much smaller movement of the tip. This will be discussed more in the Calibration section. To control the linear actuator, we used LabVIEW.

4.2 LabVIEW

LabVIEW is a graphical programming language that creates virtual instruments to control real lab instruments. Code is written in a web that resembles a circuit diagram. The programmer is able to follow the logic of the program by seeing how each of the commands are strung together. The program we wrote in LabVIEW, shown in Figure 6, allowed us to automate the approach and scanning mechanism. First, the program will check whether the tip is close enough to scan (there is a measurable tunneling current). If the tip is too far away, the computer will lower the actuator down by $0.1\mu m$ and then check again. When the tip is close enough, we click a virtual button in the program to begin the scan. Using a virtual button rather than a mechanical one on the STM's circuit board (as Chris had designed) removed the possibility of tip crashes. When the scan begins, LabVIEW will begin collecting the x, y, and z voltage measurements from a data acquisition device.
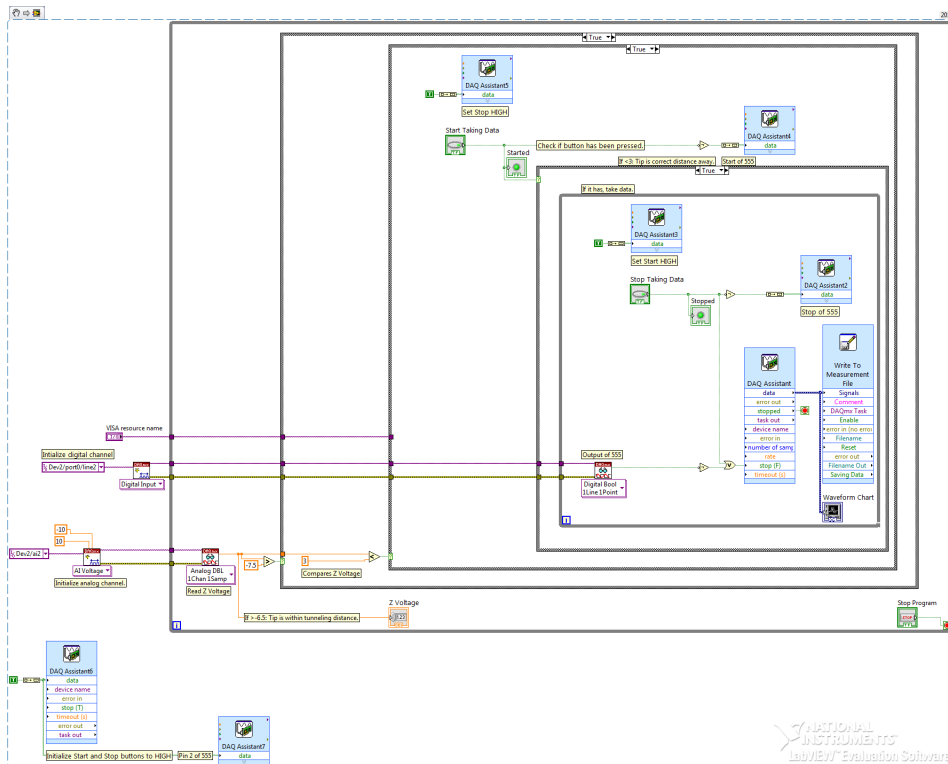
Figure 6: Screenshot of the approach and scanning code in LabVIEW.

In Figure 6, the large boxes are commands that check if a statement is true. The largest box will continue running the code within it until a stop button is pressed by the user (bottom right-hand corner). The next two loops will check whether the voltage is within the tunneling range of about $-8V$ to $8V$. If the tip is the correct distance away, the next loop will check whether the "Start Taking Data" button has been pressed. If it has, the x and y voltages will begin changing and the STM will begin scanning and collecting data. Figure 7 shows the interface used for controlling the tip approach and scanning.
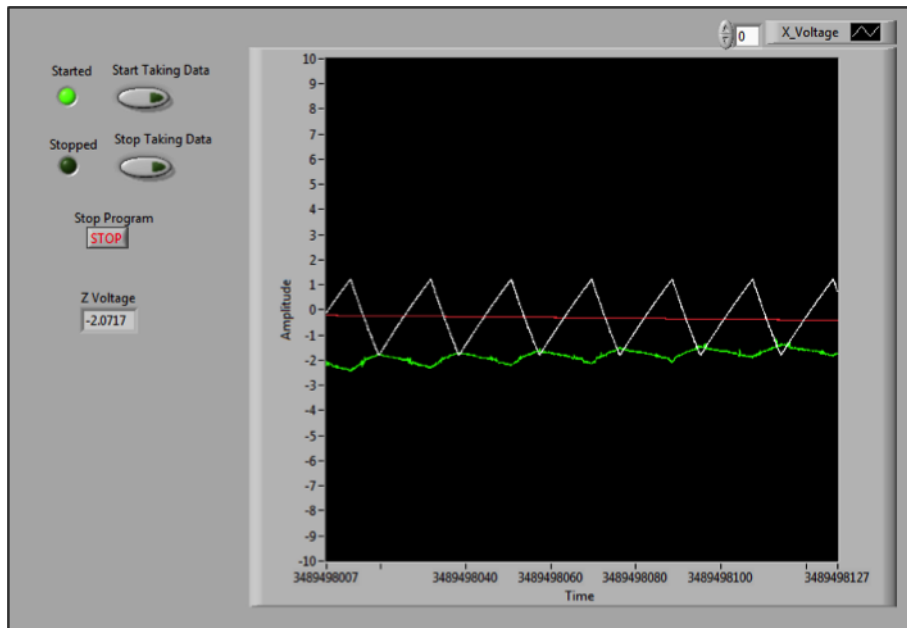
Figure 7: Screenshot of the front panel in LabVIEW. On the left are the digital buttons to begin and end scanning. The chart plots the x, y, and z voltages as the tip scans across the surface.

5 Calibration

The STM measures the voltages that are applied to the piezo, not the distances that the tip moves. There are two steps for converting the data from voltages into distances. The first step is geometrical. By looking at the geometry of the STM, we can determine how far the tip moves when the linear actuator moves a known distance. The second step is experimental. This involves determining the change in voltage as the actuator moves a known distance. If we know the change in voltage resulting from a change in actuator height, and we know the relationship between the change in actuator height and the change in tip height, we can come up with a conversion factor that relates the z voltage applied to the piezo and the change in tip height.

5.1 Z Calibration

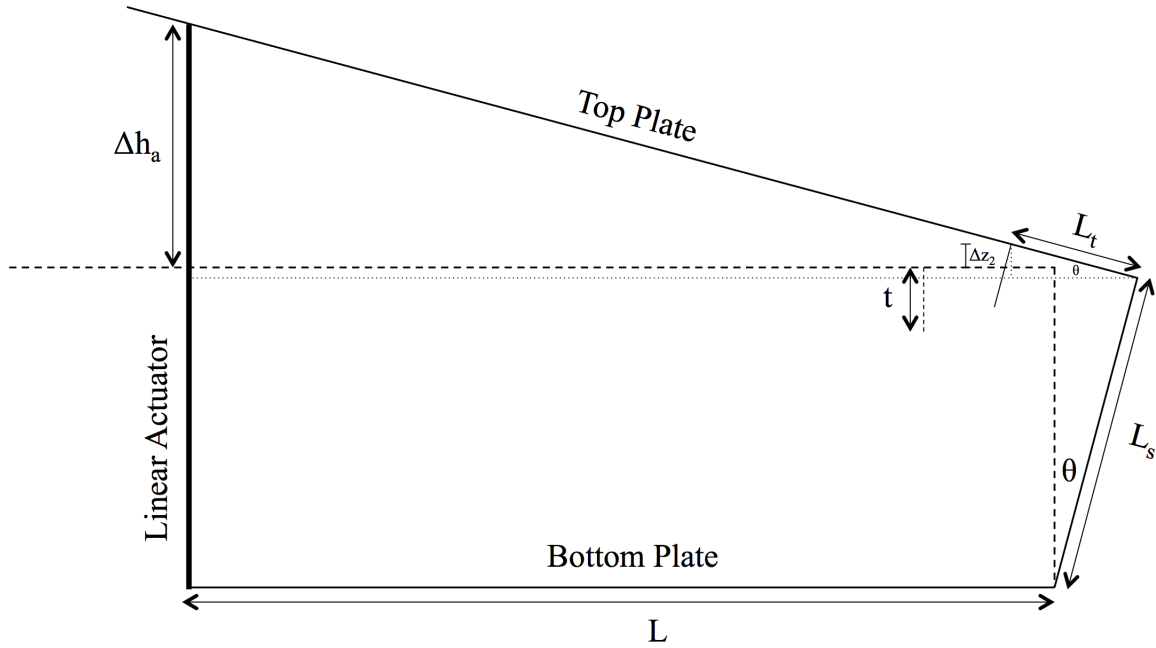### 5.1.1 Determining the Actuator Distance to Tip Distance Relationship

Figure 8: Geometrical view of tip approach. t is the length of the tip, L_s is the length of the coarse approach screw, and L_t is the distance between the tip and the coarse approach screw. θ is the angle that the top plate makes relative to the bottom plate.

The geometry of the STM is presented in Figure 8. We will assume the tip is perpendicular to the surface when the top plate is parallel with the bottom plate. When we move the actuator down a distance Δh_a to horizontal, the tip will move in two ways. First, the base of the tip will descend as the top plate is lowered. Second, the tip will swing down as the angle between the top plate and horizontal decreases. The swinging movement of the tip is shown in Figure 9.
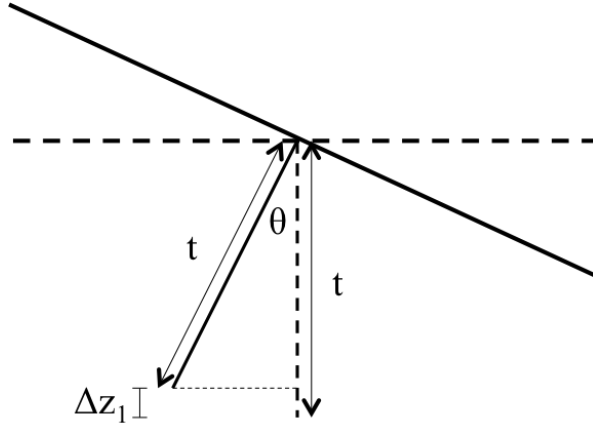
Figure 9: The tip swings through an angle θ, the same angle the top plate makes with the bottom plate.

When the top plate is raised an angle θ, the end of the tip of length t swings up a distance

$$\Delta z_1 = t(1 - \cos(\theta)). \qquad (17)$$

The change in height of the base is more involved and is derived in the appendix. The problem involves solving a system of equations for the two unknowns, Δz_T and θ. The orientation (shown in Figure 15 in the appendix) of the tip must also be taken into account. Solving the quadratic equation yields the change in tip height resulting from a change in actuator height between an arbitrary height h and horizontal. Finding the change in tip height between two arbitrary actuator height involves subtracting the change in tip height when the actuator moves between a height h_2 and horizontal from the change in tip height when the actuator moves between a height h_1 and horizontal. The resulting equation is

$$\Delta T = \frac{\Delta h(L_t L + L_s(L_s - t))}{L^2 - L_s^2} \mp$$
$$\frac{(L_s(L_t + L) - tL)(\sqrt{L^2 - L_s^2 + h_2^2} - \sqrt{L^2 - L_s^2 + h_1^2})}{L^2 - L_s^2}. \qquad (18)$$

Equation 18 allows us to determine the change in tip height using the initial and final actuator heights. We measured the constants to be: $L = 11.054$cm, $L_t = 0.35$cm, $L_s = 1.4$cm, $h_2 = 1.661$cm, and $\Delta h = 0.001875$cm.

5.1.2 Determining the Voltage to Actuator Distance Relationship

To determine the voltage-distance conversion factor, we moved the actuator by a known amount and measured the change in voltage. We measured the initial actuator height (h_1) and the final actuator height (h_2) and substituted these values into Equation 18 to find the corresponding change in tip height. Because it is difficult to measure a change in voltage from a small movement of the linear actuator, we moved the linear actuator down by a larger distance

with step sizes of $0.1\mu m$ every $2.27s$. We then measured the total change in voltage and divided by the distance the actuator moved.

We took two sets of data, one with the actuator moving down and another with the actuator moving up. Figure 10 shows the steps of the linear actuator as it moves down and the corresponding change in voltage ΔV_z for each step.
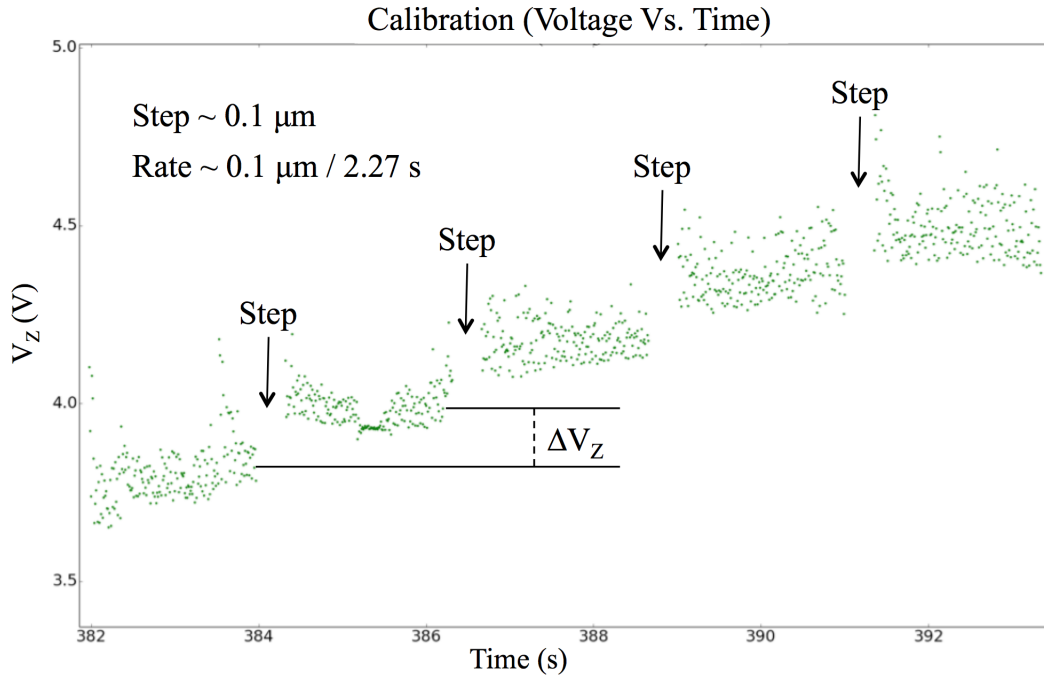

Figure 10: Individual steps of the linear actuator. The uncertainty in ΔV_z is about $0.2V$.

The linearity of the data looks promising, but upon looking at our entire data set, we found that on the mid-scale, the data was nonlinear. Figure 11 shows the complete sets of data for the forwards and backwards runs.
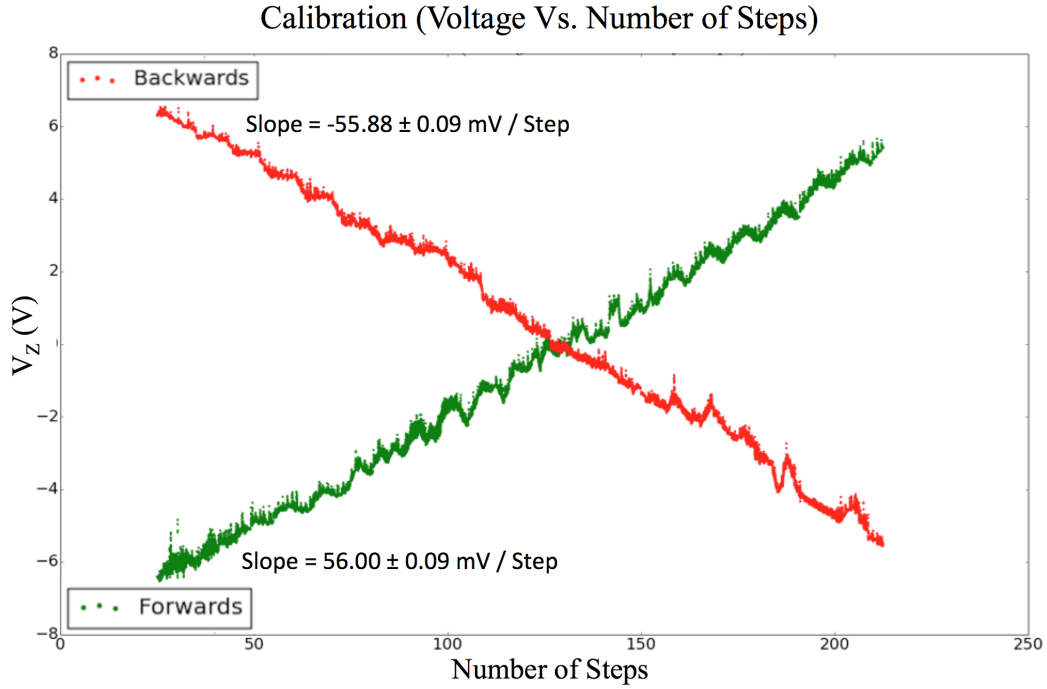
Figure 11: Data for calibration runs.

On the large scale, the data is linear and the slopes of the forwards and backwards runs agree with each other. The mid-range oscillations of the voltage may result from residue on the linear actuator or the linear actuator rotating as it moves. Because the oscillations were periodic, they did not affect the linearity of our data. Using the results from section 5.1 and 5.2, we can come up with a conversion for the z direction,

$$\frac{\Delta V_z}{\Delta T} \approx 12.93 V/\mu m. \tag{19}$$

5.2 X and Y Calibration

To determine the conversion for the x and y voltages, we need to look at the geometry of the piezo, shown in Figure 12.
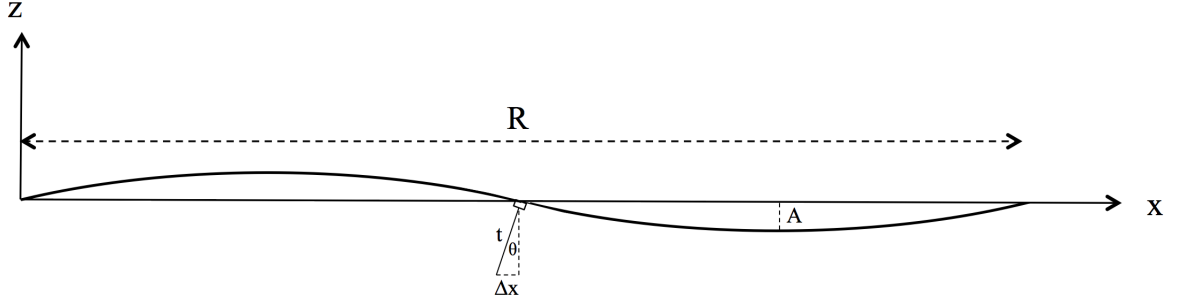
Figure 12: Geometric view of the piezo.

To find a numerical answer, we incorporated an order of magnitude approximation. When a voltage is applied to the piezo, we can approximate the surface of the deformed piezo as a sine wave. The height at any point is given by

$$z = A \sin\left(\frac{2\pi x}{R}\right),$$
(20)

where A is the maximum amplitude of the sine wave (or maximum displacement of the piezo from equilibrium) and R is the distance across the piezo. The actual deformation would probably depend on the z voltage. It could be found by scanning a sample with surface features of a known size.

Taking a derivative of Equation 20 with respect to x gives

$$\frac{dz}{dx} = \frac{2\pi A}{R} \cos\left(\frac{2\pi x}{R}\right),$$
(21)

which is the slope of the piezo. Evaluating this at $x = R/2$ yields $-\frac{2\pi A}{R}$. The angle between the deformed piezo and the x axis is equal to the angle between the tip and a vertical axis. Thus, the slope at $x = R/2$ is equal to $\tan(\theta)$. Equating these two slopes gives

$$\tan(\theta) = \frac{2\pi A}{R}.$$
(22)

From Figure 12 we also have

$$\tan(\theta) = \frac{\Delta x}{t \cos(\theta)}.$$
(23)

After setting these two equations equal and using the small angle approximation $(\cos(\theta) \approx 1)$, we find

$$\Delta x \approx \frac{2\pi A t}{R},$$
(24)

where $A \approx \frac{1}{2}\Delta t$. A is the amplitude of the piezo when it is deformed by an x or y voltage, which is approximately half the amplitude when the same voltage is applied in the z direction such as in Figure 15 in the appendix. We can now find a conversion factor for the x and y directions,

$$\left(\frac{x}{Volts}\right) = \left(\frac{y}{Volts}\right) = \frac{\pi t}{R}\left(\frac{z}{Volts}\right). \tag{25}$$

Using the result from Equation 19 and the slopes in Figure 11, we found the following conversion,

$$\frac{\Delta V_x}{\Delta T} = \frac{\Delta V_y}{\Delta T} \approx 9.78 V/\mu m \tag{26}$$

6   Analysis

After receiving the data from LabVIEW and converting the voltages into distances, we wrote a Python program to create a three dimensional map of the surface. The program uses a Radial Basis Function (RBF) interpolation and is presented in the appendix. We began with a wire frame plot of the data and then used the built-in RBF method to interpolate between data points. Below are examples of a graphite surface and a gold surface using the Python program.
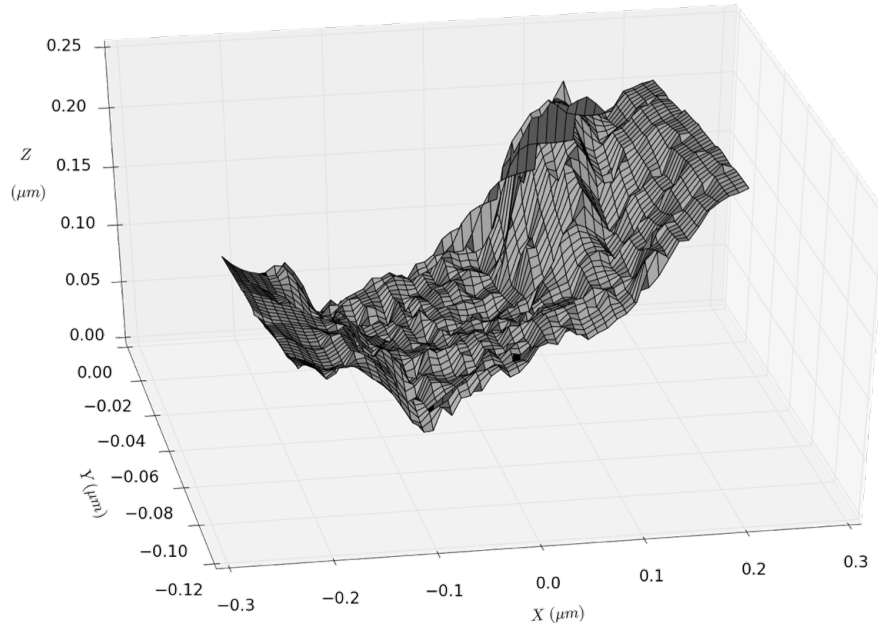

Figure 13: Plot of a graphite surface.

We were able to reproduce the graphite surface multiple times. Because of the large changes in height, we suspect that we scanned over a region where we crashed the tip.
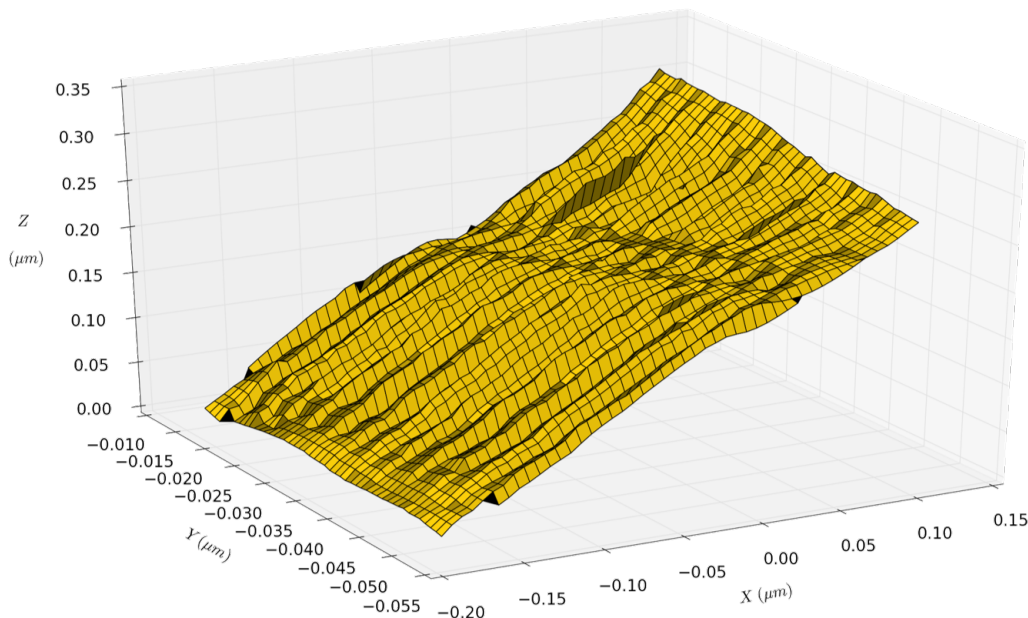
Figure 14: Plot of a gold surface.

The gold surface is more uniform than the graphite surface and consists of equally spaced ridges along the surface. We believe the tip was scraping the surface while it was scanning because the ridges are aligned with the x axis. From Figure 13 and Figure 14, we can determine a rough resolution of tens of nanometers.

7   Conclusion

We have successfully automated and calibrated the STM. We hope to use this STM in an advanced laboratory course to introduce students to quantum tunneling. The STM provides a visual demonstration of quantum tunneling and will give students experience in LabVIEW. We have begun construction on a scanning capacitance microscope (SCM), which measures the capacitance between a tip and a surface as the tip is scanned across it. We designed the two microscopes so that a student could toggle between STM mode and SCM mode. Future work involves designing a lab activity for students. In addition, we could get a calibrated sample to work out a voltage-distance relation and compare that with the one we found geometrically.

8   Acknolwedgements

We would like to acknowledge Stan Schroeder for assisting us with soldering. We would also like to acknowledge Dr. Alan DeWeerd for giving us pointers and helping us write code in LabVIEW. We would like to thank Chris Adams

A Z Calibration

From Figure 8,

$$\Delta z_2 = L_t \sin(\theta) - L_s(1 - \cos(\theta)). \tag{27}$$

The total change in height of the tip is the sum of the movement of the base and the swinging movement of the tip,

$$\Delta z_T = \Delta z_1 + \Delta z_2 = (t - L_s)(1 - \cos(\theta)) + L_t \sin(\theta). \tag{28}$$

To solve for the two unknowns (Δz_T and θ) we can obtain another equation from Figure 8,

$$\tan(\theta) = \frac{\Delta h_a + L_s(1 - \cos(\theta))}{L + L_s \sin(\theta)}. \tag{29}$$

Simplifying gives

$$\Delta h_a + L_s = L_s \sec(\theta) + L \tan(\theta). \tag{30}$$

Δz_T in Equation 28 is the distance the tip moves relative to horizontal. To find a conversion, we need the distance Δt the tip moves relative to the piezo. Instead of the base of the tip moving because of the lowering of the plate, it is easier to imagine the piezo extending, shown in Figure 15. The distance the tip moves perpendicular to the piezo is the distance related to the applied z voltage.
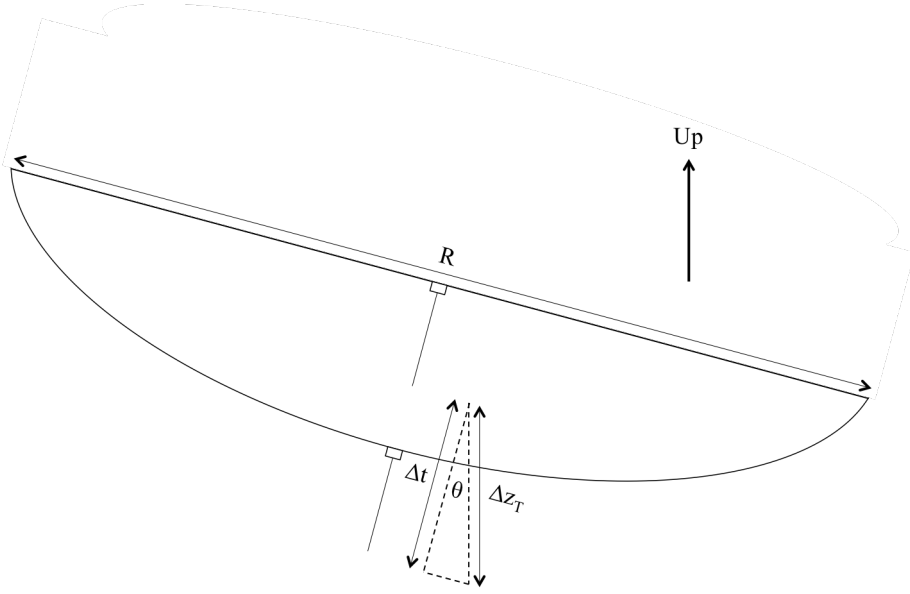
Figure 15: If the tip moves an amount Δz_T relative to horizontal, it will move an amount Δt relative to the piezo.

From Figure 15,

$$\Delta t = \frac{\Delta z_T}{\cos(\theta)}. \tag{31}$$

Substituting Equation 28 into Equation 31 yields

$$\Delta t = (t - L_s)(\sec(\theta) - 1) + L_t \tan(\theta). \tag{32}$$

We now have two equations (30 and 32) and two unknowns (θ and Δt). Solving Equation 30 for $\tan(\theta)$ and squaring both sides yields

$$\sec^2(\theta) - 1 = \frac{\Delta h_a^2 + 2\Delta h_a L_s(1 - \sec(\theta)) + L_s^2(1 - \sec^2(\theta))^2}{L^2}, \tag{33}$$

where I have used $\tan^2(\theta) = \sec^2(\theta) - 1$. We can re-write the left side using $\sec^2(\theta) - 1 = (\sec(\theta) - 1)^2 + 2(\sec(\theta) - 1)$. The goal is to obtain a quadratic equation for the quantity $\sec(\theta) - 1$. Multiplying by L^2 on both sides yields

$$L^2(\sec(\theta) - 1)^2 + 2L^2(\sec(\theta) - 1) = \Delta h_a^2 - 2\Delta h_a L_s(\sec(\theta) - 1) + L_s^2(\sec^2(\theta) - 1)^2, \tag{34}$$

where I have used $\sec(\theta) - 1 = -(1 - \sec(\theta))$, and $(\sec(\theta) - 1)^2 = (1 - \sec(\theta))^2$. We can put this in quadratic form by collecting powers of $\sec(\theta) - 1$,

$$(L^2 - L_s^2)(\sec(\theta) - 1)^2 + 2(L^2 + \Delta h_a L_s)(\sec(\theta) - 1) - \Delta h_a^2 = 0. \tag{35}$$

Using the quadratic formula and simplifying gives

20

$$\sec(\theta) - 1 = \frac{-(L^2 + \Delta h_a L_s) \pm L\sqrt{(L^2 - L_s^2) + (\Delta h_a + L_s)^2}}{L^2 - L_s^2}. \tag{36}$$

We can substitute Equation 36 into Equation 32 and simplify. After defining the new variable $h \equiv \Delta h_a + L_s$ we get

$$\Delta t = \frac{\mp(L_s(L_t + L) - tL)\sqrt{L^2 - L_s^2 + h^2} + h(L_t L + L_s(L_s - t))}{L^2 - L_s^2} + $$
$$\frac{-L_s^3 + L_s^2 + L^2(L_s - t)}{L^2 - L_s^2}. \tag{37}$$

We defined Δh_a as the actuator height above horizontal. Thus Δt is a measure of the tip displacement (relative to the piezo) between the top plate at an arbitrary height and horizontal. What we want is the tip displacement between two arbitrary heights of the linear actuator. If h_1 is the initial height of the actuator and it moves an amount Δh, then $h_2 = h_1 + \Delta h$ is the final height of the actuator. $\Delta T = \Delta t_2 - \Delta t_1$ is the corresponding change in tip displacement. Substituting h_1 and h_2 into Equation 37 and subtracting the two equations gives ΔT, the change in tip height perpendicular to the piezo between to arbitrary actuator heights,

$$\Delta T = \frac{\Delta h(L_t L + L_s(L_s - t))}{L^2 - L_s^2} \mp $$
$$\frac{(L_s(L_t + L) - tL)(\sqrt{L^2 - L_s^2 + h_2^2} - \sqrt{L^2 - L_s^2 + h_1^2})}{L^2 - L_s^2}. \tag{38}$$

B Tip Preparation

To create tips, tungsten (W) wire is electrochemically etched in a solution of NaOH. When a voltage is applied across the tungsten wire and an electrode, tungsten begins flaking off. Within a few minutes, the tip is etched to a sharp point. Once the tip is etched, we rinse it off with distilled water to remove any contamination. We can be sure that there is a single atom at the end of the tip, but the resolution of each tip is unpredictable. A review of tip treatment in STM literature revealed a few facts:[22]

1. Atomic resolution could happen unexpectedly after a certain amount of time.

2. Crashed tips can recover to maintain atomic resolution.

3. The tip can undergo changes during scanning which affect the resolution.

4. A mechanically cut tip can often work just as well as a chemically etched one.

In general, there is no way to guarantee the tip will give the best possible resolution. For our purposes, it is not as crucial that the tip be ideal because we are not able to obtain atomic resolution.

C Surface Plotting Program

```python
#Import modules
import scipy as sp
import scipy.interpolate
import numpy as np
#from scipy.interpolate import griddata
from matplotlib.mlab import griddata
from mpl_toolkits.mplot3d.axes3d import *
from numpy import *
from pylab import *

#Read Data from file
x, y, z = loadtxt('Graphite5.7XY.txt', unpack=True, usecols=[0,1,2])

znew = z-min(z)

Zdist = znew*0.0773
xdist = x*0.1022
ydist = y*0.1022

#Gridding and Interpolating Data
sp.interpolate.Rbf(xdist,ydist,Zdist)
xi = np.linspace(min(xdist), max(xdist))
yi = np.linspace(min(ydist), max(ydist))
X, Y = np.meshgrid(xi, yi)

Z = griddata(xdist, ydist, Zdist, xi, yi)

#Graphing Data
fig = plt.figure()
ax = Axes3D(fig)

surf = ax.plot_surface(X, Y, Z, rstride=1, cstride=1, linewidth=1,
antialiased=True, color = '0.75')
ax.set_xlabel('$X$ $(\mu m)$', fontsize = 24)
ax.set_ylabel('$Y$ $(\mu m)$', fontsize = 24)
ax.set_zlabel('$Z$ \n \n $(\mu m)$', fontsize = 24)
plt.tick_params(labelsize=24)
ax.zaxis.set_rotate_label(False)
title('$Graphite \ Sample$', fontsize = 30)
```

Notes

[1]G. Binnig et al., "Surface Studies by Scanning Tunneling Microscopy," *Phys. Rev. Lett.* **49** (1), 57-61 (1982).

[2]D. A. Bonnell, *Scanning Probe Microscopy and Spectroscopy: Theory, Techniques, and Applications*, 2nd ed. (Wiley-VCH, New York, NY, 2001), p. 3.

[3]J. A. Stroscio and W. J. Kaiser, *Scanning Tunneling Microscopy*, in *Methods of Experimental Physics*, Vol. 27. (Academic Press, San Diego, CA, 1993), p. 31.

[4]C. Bai, *Scanning Tunneling Microscopy and Its Applications*, 2nd ed. (Springer, Berlin, Germany, 2000), p. 2.

[5]R. Wiesendanger, *Scanning Prove Microscopy and Spectroscopy: Methods and Applications*, (Cambridge University Press, Cambridge, England, 1994), pp. 470-471.

[6]C. Bai, *Scanning Tunneling Microscopy and Its Applications*, p. 279.

[7]D. Stievenard, "Microscopic characterization of defects using scanning tunneling microscopy," *Mat. Sci. Eng. B-Solid* **B71** (1-3), 120-127 (2000).

[8]S. Hla, "Scanning tunneling microscopy single atom/molecule manipulation and its application to nanoscience and technology," *J. Vac. Sci. Technol. B* **23**, 1351-1360 (2005).

[9]C. J. Chen, *Introduction to Scanning Tunneling Microscopy*, 1st ed. (Oxford University Press, New York, 1993), p. 5.

[10]C. J. Chen, *Introduction to Scanning Tunneling Microscopy*, 1st ed. (Oxford University Press, New York, 1993), p. 5.

[11]D. J. Griffiths, *Introduction to Quantum Mechanics*, 2nd ed. (Pearson Prentice Hall, Upper Saddle River, NJ, 2005, p. 82.

[12]D. J. Griffiths, *Introduction to Quantum Mechanics*, p. 322.

[13]J. Tersoff, D. R. Hamann, "Theory and Application for the Scanning Tunneling Microscope," *Phys. Rev. Lett.* **50** (25), 1998 (1983).

[14]C. J. Chen, *Introduction to Scanning Tunneling Microscopy*, p. 75.

[15]J. Bardeen, "TUNNELLING FROM A MANY-PARTICLE POINT OF VIEW," *Phys. Rev. Lett.* **6** (2), 57-59 (1961).

[16]J. Tersoff and D.R. Hamann, "Theory and Application for the Scanning Tunneling Microscope," *Phys. Rev. Lett.* **50** (25), 1998-2001 (1983).

[17]C. J. Chen, *Introduction to Scanning Tunneling Microscopy*, p. 61.

[18]C. J. Chen, *Introduction to Scanning Tunneling Microscopy*, p. 61.

[19]www.parkAFM.com

[20]www.parkAFM.com

[21]C. J. Chen, *Introduction to Scanning Tunneling Microscopy*, p. 237.

[22]C. J. Chen, *Introduction to Scanning Tunneling Microscopy*, pp. 281-282.